MATERIALS CHEMISTRY
FRONTIERS

RESEARCH ARTICLE

View Article Online
View Journal | View Issue

Cite this: *Mater. Chem. Front.*, 2019, **3**, 656

The design of Janus black phosphorus quantum dots@metal–organic nanoparticles for simultaneously enhancing environmental stability and photodynamic therapy efficiency†

Da Zhang, ‡[abc] Ziguo Lin,‡[acd] Shanyou Lan,[acd] Haiyan Sun,*[e] Yongyi Zeng *[abcd] and Xiaolong Liu *[abc]

Although newly-developed black phosphorus quantum dots (BPQDs) with unique photocatalytic properties have attracted much attention for biomedical applications, especially phototherapy, the environmental instability and weak photocatalytic activity of BPQDs remains a considerable challenge preventing their clinical application. Herein, we have designed new Janus nanoparticles (J-MOPs) based on BPQDs and tetrahydroxyanthraquinone (THQ)–Cu metal–organic particles (MOPs) to simultaneously improve the environmental stability and photocatalytic activity for the PDT treatment of cancers. The J-MOPs were simply assembled from BPQDs and THQ *via* Cu-mediated P–Cu–THQ "host–metal–guest" coordination effects. The encapsulation of BPQDs inside J-MOPs and P–Cu bonds effectively isolated BPQDs from water–air and occupied the P lone-pair electrons, respectively, to improve the stability of BPQDs. Furthermore, the dramatic electron–hole separation and migration abilities of J-MOPs increased the reactivity toward O_2, which enhanced singlet oxygen ($^1O_2$) generation against cancers compared with BPQDs alone when exposed to 670 nm laser irradiation. Intriguingly, tumor acid-triggered J-MOPs degradation resulted in the release of Cu^{2+} ions that further served as a Fenton-like agent to generate $^{\bullet}OH$ from H_2O_2, which enhanced the antitumor effects of the J-MOPs. Therefore, we have highlighted the potential of J-MOPs as a photocatalyst for photodynamic cancer therapy.

Received 5th December 2018,
Accepted 13th February 2019

DOI: 10.1039/c8qm00623g

rsc.li/frontiers-materials

Introduction

Black phosphorus nanosheets (BPNs)/quantum dots (BPQDs) are two-dimensional (2D) materials that have attracted extensive interests in recent years owing to their unique anisotropic layered structure, high electron mobility, proper band gap (spanning from 0.3 eV (bulk value) to ~2.1 eV (monolayer value)) and excellent photocatalytic properties.[1–5] Especially in biomedical fields, the unique photocatalytic activity of BPNs/BPQDs with smaller nano-sizes (<10 nm) could be used as safety photosensitizer agents for cancer photodynamic therapy owing to their extremely high biosafety and minimized side effects. These include effective elimination of BPNs/BPQDs by the renal and liver systems[6–11] and biodegradation into phosphorus to serve as a nutrient in the body. However, the inherent instability of BPNs/BPQDs under water–air conditions seriously hinders their biomedical applications. Furthermore, the weak absorption of BPNs/BPQDs in the optical windows of biological tissues and low photocatalysis activity in hypoxic microenvironment (TME) significantly limit their applications in cancer treatment.[12–15] Therefore, the development of an effective strategy to simultaneously improve the environmental stability and maximize the photocatalytic activity of BPNs/BPQDs is urgently needed to further explore its applications in biosystems.

Some strategies to enhance the environmental stability of BPNs/BPQDs have been developed in recent years. One strategy involved occupying the phosphorus lone-pair electrons in BPNs/BPQDs by dropping metal ions, such as Ti and lanthanides (Ln = Gd, Tb, Eu, Nd, *etc.*), onto them.[16–20] Another strategy involved adsorbing organic materials/inorganic molecules onto the surface of BPNs/BPQDs, including peptides, dyes, and polydopamine biomaterials.[21–25] The third approach is forming self-assembled or cooperated nanostructures, such as PLGA,

[a] *The United Innovation of Mengchao Hepatobiliary Technology Key Laboratory of Fujian Province, Mengchao Hepatobiliary Hospital of Fujian Medical University, Fuzhou 350025, P. R. China. E-mail: xiaoloong.liu@gmail.com*
[b] *Mengchao Med-X Center, Fuzhou University, Fuzhou 350116, P. R. China*
[c] *The Liver Center of Fujian Province, Fujian Medical University, Fuzhou 350025, P. R. China*
[d] *Liver Disease Center, The First Affiliated Hospital of Fujian Medical University, Fuzhou 350005, P. R. China. E-mail: lamp1973@medmail.com.cn*
[e] *Department of Anesthesiology, Beijing Anzhen Hospital, Capital Medical University, Beijing 100029, P. R. China. E-mail: 2254103187@qq.com*
† Electronic supplementary information (ESI) available. See DOI: 10.1039/c8qm00623g
‡ These authors contributed equally to this work.

to isolate BPQDs.[26,27] Furthermore, to enhance the photocatalysis activity of BPNs/BPQDs, the electromagnetic near-field enhancement mechanism of plasmonic metals has been used to boost singlet oxygen generation, while another strategy is increasing the NIR absorption of BPNs/BPQDs or enhancing their local-field plasmonic effect using gold nanoparticles through the localized surface plasmon resonance (LSPR) effect.[28,29] Furthermore, the fabrication of nanohybrids with electron–hole separation and migration abilities enhanced the reactivity with H_2O and O_2 to generate $^1O_2$ through the effect of photogenerated electrons and holes.[2,30–32] Recently, so-called Janus nanoparticles (JNPs) have simultaneously presented two different sets of material and chemical properties in an "all-in-one" platform, which might be an excellent and effective strategy for designing nanohybrids for cancer therapy.[33–41] To date, the construction of JNPs from metal–organic nanoparticles and BPQDs to simultaneously improve the environmental stability and enhance $^1O_2$ generation ability for PDT treatment has yet to be reported.

In this study, we designed new Janus nanoparticles (J-MOPs) based on BPQDs and THQ–Cu MOPs to simultaneously improve the environmental stability and ROS generation for enhancing PDT efficiency (Fig. 1). In our design, the J-MOPs were simply self-assembled from THQ and BPQDs by Cu^{2+}-mediated coordination through Cu–P and THQ–Cu bonds. The advanced nanostructure exhibited several features, as follows: (i) excellent water–air stability of the encapsulated BPQDs due to Cu–P bonds occupying the phosphorus lone-pair electrons and isolating the BPQDs from air and water; (ii) significantly enhanced ROS generation owing to the electron–hole separation and migration ability of the J-MOPs nanostructure; and (iii) effective oxidative stress injury to tumor cells and excellent PDT antitumor effects both *in vitro* and *in vivo*.

Results and discussion

The J-MOPs were designed and synthesized as shown in Fig. 2A. Briefly, the prefabricated BPQDs, THQ organic dye, and Cu^{2+} ions were first mixed in aqueous solution (pH 7.4) and then vigorously stirred for 1 h. After centrifugation, the J-MOPs were obtained. The size and morphology of the prepared BPQDs and J-MOPs were characterized by transmission electron microscopy (TEM). As shown in Fig. 2B and C, the BPQDs showed a narrow size distribution of around 6 ± 2.8 nm with a typical dot morphology similar to those reported previously.[1–8] The J-MOPs showed an average size of 25 ± 6.9 nm in diameter, with the BPQDs embedded inside the THQ–Cu MOPs framework corresponding to the enlarged TEM image. The energy band (LUMO) and band gap (E_g) of THQ were calculated from the X-ray photoelectron spectroscopy and absorption spectra, respectively (Fig. 2D and E). The HOMO of THQ was calculated to be 5.61 eV using the following equation: LUMO = HOMO − E_g. Raman spectra suggested that J-MOPs consisted of BPQDs with three specific prominent peaks, including one out-of-plane phonon mode (A_g^1) at 361.2 cm^{-1} and two in-plane modes, B_g^2 and A_g^2, at 439.2 cm^{-1} and 466.5 cm^{-1}, respectively.[1–8] Furthermore, THQ showed two prominent peaks at 466.5 cm^{-1} and 557 nm^{-1} (Fig. 2F). Notably, the THQ signals from J-MOPs at 439.2 cm^{-1}, 466.5 cm^{-1}, and 557.4 cm^{-1} were higher than those of THQ alone, which might be due to surface-enhanced Raman scattering. Interestingly, the A_g^1 mode of J-MOPs at 361.2 cm^{-1} was right-shifted to 370.4 cm^{-1} and much lower than that of the BPQDs, which might be due to the Cu–P and Cu–THQ coordination bond interactions. To confirm this result, X-ray photoelectron spectroscopy (XPS) was performed. As shown in Fig. S1 (ESI†), the XPS

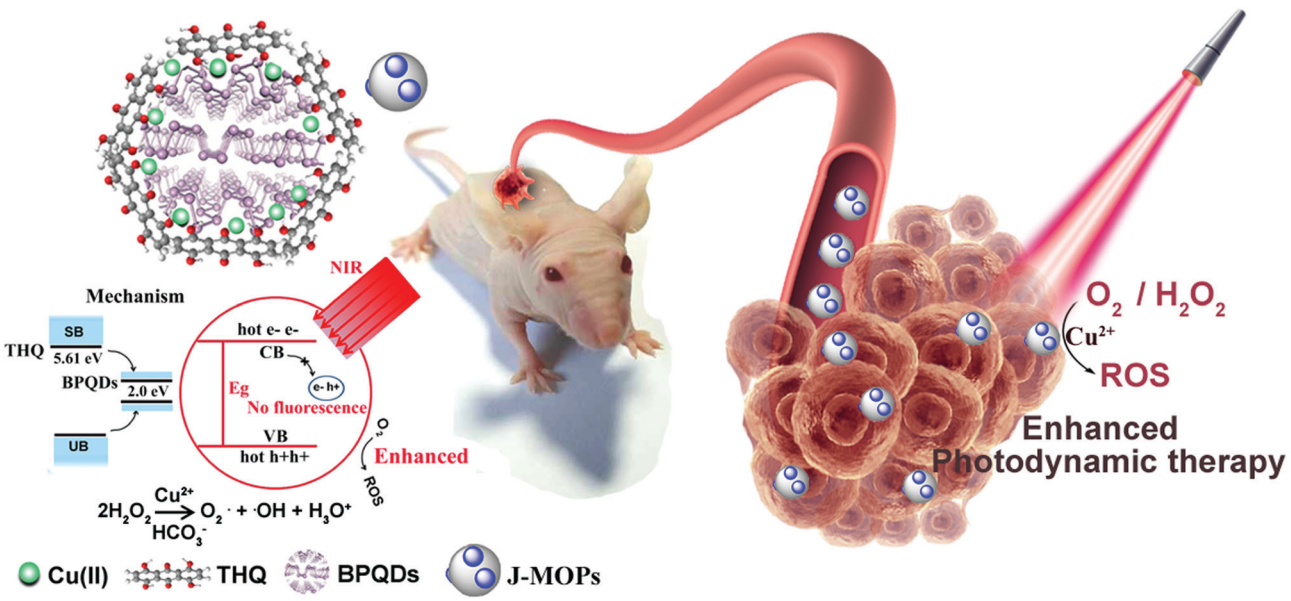

Fig. 1 Schematic illustration of the preparation and mechanism of Janus nanoparticles (J-MOPs). J-MOPs were simply assembled from BPQDs, Cu^{2+} ions, and THQ using a one-step method. The J-MOPs exhibited excellent water–air stability owing to the effective encapsulation of BPQDs inside J-MOPs and occupation of phosphorus lone-pair electrons in P–Cu bonds, and significantly enhanced ROS generation ability resulting from the electron–hole separation and migration ability of the J-MOPs. Meanwhile, Cu^{2+} acted as a Fenton-like agent. Upon NIR laser irradiation, the enhanced ROS generation synergized with the Fenton-like activity of Cu^{2+} ions to effectively inhibit tumor growth for cancer phototherapy.

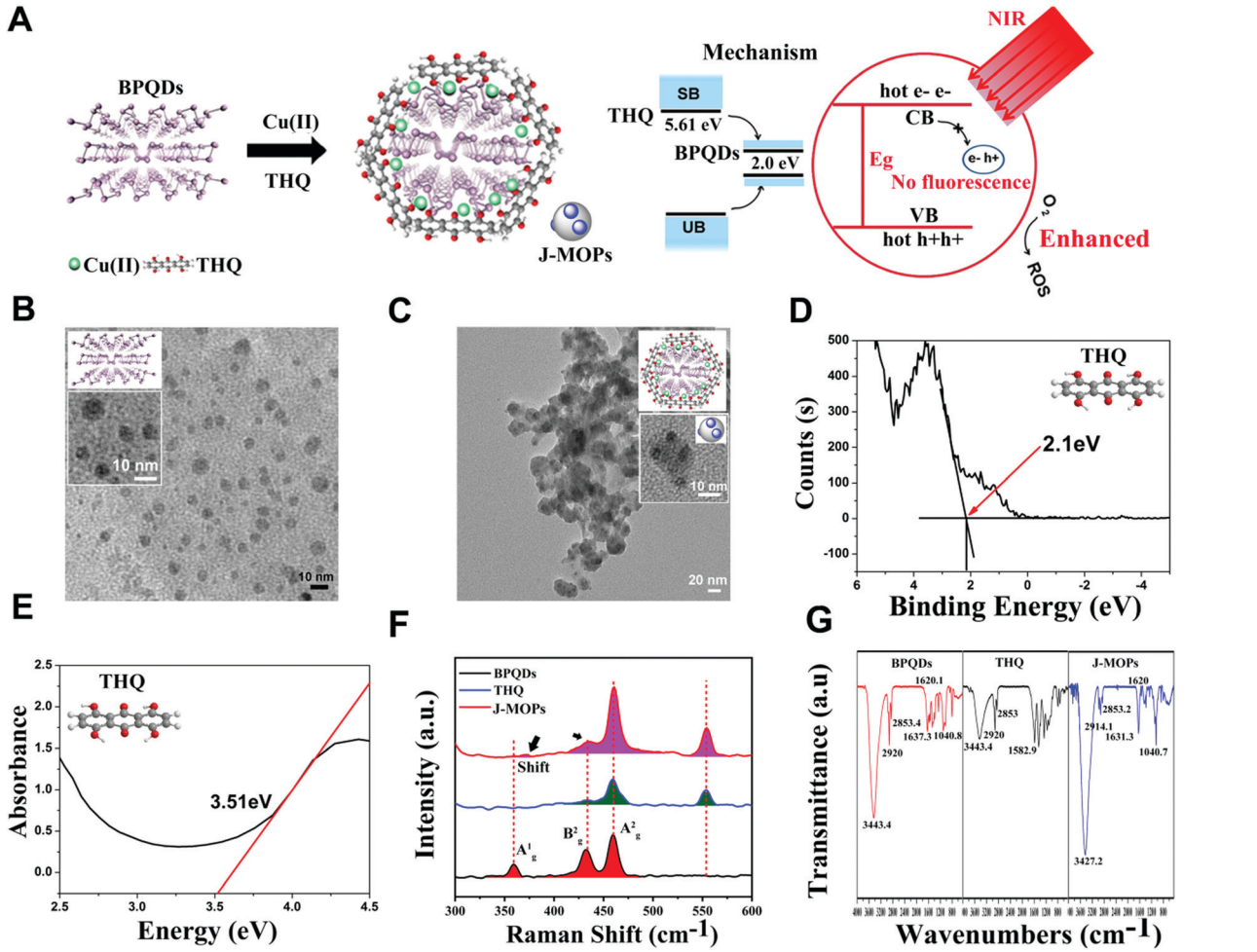

Fig. 2 (A) Schematic illustration of the process for synthesizing J-MOPs and the mechanism of enhanced ROS generation. (B) TEM images of BPQDs and (C) J-MOPs, inset picture and diagram present enlarged images of BPQDs and J-MOPs. (D) X-ray photoelectron spectroscopy and (E) absorbance spectra of THQ. (F) Raman spectra of BPQDs, THQ, and J-MOPs. (G) FTIR spectra of THQ, BPQDs, and J-MOPs.

spectrum of J-MOPs showed a sub-band at P_{2p} 130.1 eV, which was attributed to Cu-bonded P. The strong peak at 532 eV of O_{1s} was attributed to hydride adsorption by THQ. XPS also showed typical $Cu2p_{3/2}$ and $Cu2p_{1/2}$ peaks with measured binding energies of 935.1 and 955.0 eV, which corresponded to Cu^{2+} on the J-MOPs. Furthermore, the J-MOPs were mainly composed of P, Cu, O, and C elements, and Cu was successfully coordinated into the BPQDs. These results were further confirmed by energy-dispersive X-ray spectroscopy (EDS), suggesting interactions between Cu–P and Cu–THQ in the J-MOPs (Fig. S2, ESI†). To further confirm the compositions of the J-MOPs, Fourier-transform infrared spectroscopy (FTIR) was performed. As shown in Fig. 2G, absorption bands at 3427.2, 2914.1, 1631.3, and 1040.7 cm^{-1} corresponded to stretching vibrations of –OH, –CH, C=C, and C–O groups, respectively indicating the existence of THQ and BPQDs in the J-MOPs. Furthermore, the weaker absorption of J-MOPs compared with that of THQ at 1620 cm^{-1} was due to the stretching vibration of the C=O groups in conjugated ketones resonating between C–O/C=O and Cu^{2+}, indicating the presence of Cu(II) in these J-MOPs.[12,42] Furthermore, the optical absorption properties of the J-MOPs and BPQDs were analyzed to confirm the existence of Cu^{2+} ions. As shown in Fig. 3A, the J-MOPs exhibited a new absorption peak at 520 nm, which was attributed to Cu^{2+} ions from the J-MOPs.[12] The J-MOPs also showed a broad absorption from 450 nm to 850 nm, which was much higher than that of the bare BPQDs, owing to the surface enhancement of THQ–Cu complexes in the π-conjugation system.

Next, the water–air and physiological stabilities of the prepared J-MOPs were investigated, respectively. As shown in Fig. 3B, the color of the J-MOPs remained brown after exposing to water–air conditions for 48 h, while the color of the bare BPQD solution faded to transparent after 48 h under the same conditions. Furthermore, ultraviolet-visible-near infrared (UV-vis-NIR) spectra were recorded, and the results clearly suggested that the absorbance of the prepared J-MOPs was very stable owing to the Cu–P bonds and the effective encapsulation of the BPQDs to isolate them from water and air. Meanwhile, the absorbance intensity of the bare BPQDs significantly decreased with increasing storage time (Fig. 3C and D). Furthermore, the J-MOPs were very stable in PBS buffer solution (pH 7.4) and medium (containing 10% FBS), compared with naked BPQDs (Fig. S3, ESI†). Next, we further evaluated the reactive oxygen species (ROS) generation

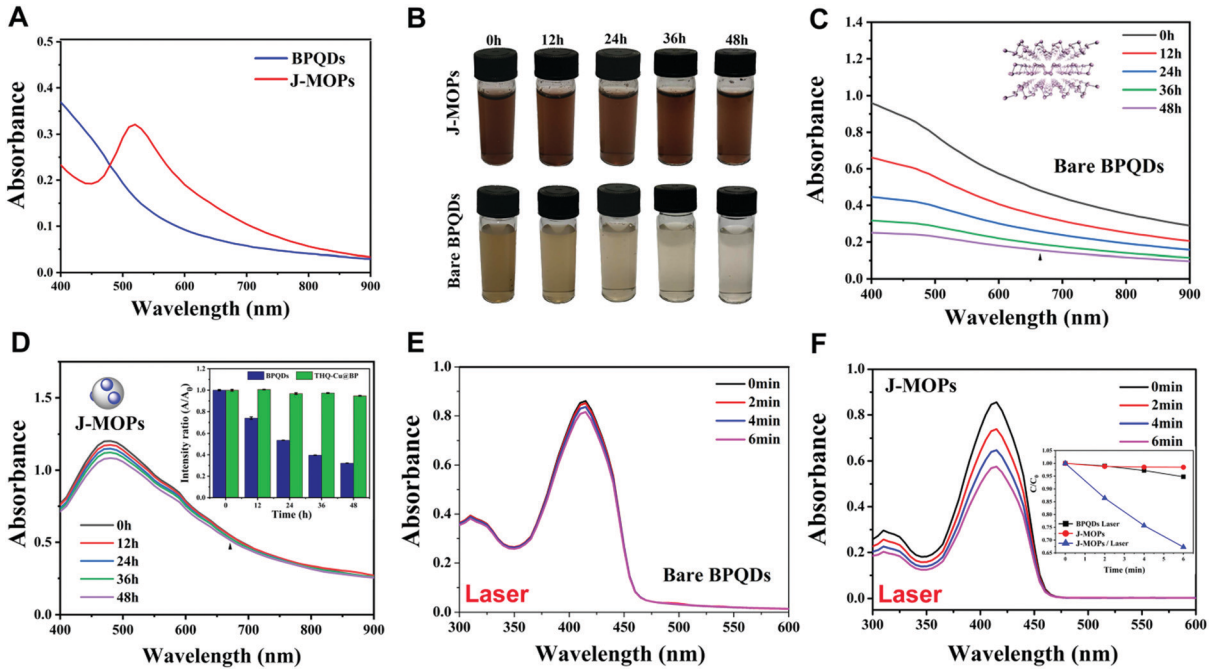

Fig. 3 (A) Absorbance of BPQDs and J-MOPs in PBS buffer; (B) optical properties and stability under ambient conditions; (C and D) absorption spectra of BPQDs and J-MOPs with the same amount of BPQDs after storing under water–air conditions for different periods. Inset in (D): variation of absorption ratios (A/A_0) at 670 nm. (E) Absorption of DPBF after photodecomposition by ROS generation in BPQDs; and (F) J-MOPs after 670 nm laser irradiation for different time periods (670 nm, 0.1 W cm^{-2}). Inset in (F) shows the normalized absorption of DPBF at 415 nm in J-MOPs and BPQDs after 670 nm laser irradiation for 0, 2, 4, and 6 min (670 nm, 0.1 W cm^{-2}).

ability of our J-MOPs using an ROS indicator (1,3-diphenylisobenzofuran, DPBF) during 670 nm laser irradiation, using the bare BPQDs as a control.[16–25] As shown in Fig. 3E and F, and Fig. S4 (ESI†), the J-MOP-encapsulated BPQDs within PBS buffer exhibited a sharp decline in DPBF absorbance in the range of 350 nm to 450 nm when exposed to 670 nm lasers with a power intensity of 0.1 W cm^{-2}. However, the bare BPQDs within PBS buffer only showed a slight decline in DPBF absorbance in the same environment and under the same laser power conditions owing to the instability and self-degradation of BPQDs under water–air conditions. Furthermore, by normalizing the absorbance at 415 nm, the absorbance of the J-MOPs decreased 6.2-fold compared with that of the BPQDs after irradiation for 6 min (Fig. 3F, inset picture). These results indicated that the ROS generation ability of our designed J-MOPs was significantly enhanced comparing with bare BPQDs, because the BPQDs could constantly donate electrons and accept holes from THQ through Cu^{2+} ions as a bridge, which led to a reduction in electron–hole recombination (Fig. S5, ESI†).[29–32] These results suggested that our J-MOPs with dramatic electron–hole separation and migration abilities could enhance the reactivity with O_2 to produce ROS. Altogether, our designed J-MOPs not only improved the stability of BPQDs, but also enhanced their ROS generation ability.

Before therapeutic applications, the cellular uptake of J-MOPs by hepatocellular carcinoma (HepG2) cells was evaluated using confocal scanning microscopy (CLSM). As shown in Fig. 4A, the THQ organic dye with red fluorescent signals (561 nm laser excitation) from J-MOPs was almost invisible in the cytoplasm of HepG2 cells after incubation for 1 h. With prolonged incubation, the red fluorescence intensity of THQ from J-MOPs was significantly enhanced in the cytoplasm of cells at 37 °C owing to the tumor acid-triggered degradation of J-MOPs, which was consistent with the characteristics of MOPs,[12,42,44] suggesting the effective uptake of J-MOPs by cancer cells. Next, we investigated the intracellular ROS generation of J-MOPs using intracellular ROS fluorescence indicator DCFH-DA after 670 nm laser irradiation. As shown in Fig. 4B, HepG2 cells alone with or without laser irradiation showed background fluorescence (green). Meanwhile, HepG2 cells treated with either bare BPQDs or the J-MOPs without laser irradiation showed no fluorescence intensity enhancements. In contrast, the green fluorescence intensity was significantly increased in J-MOPs-treated cells after 670 nm laser irradiation for 5 min (0.1 W cm^{-2}). Notably, HepG2 cells treated with BPQDs at the same concentration showed relatively weak fluorescence owing to the degradation and instability of BPQDs during incubation. These results indicated that our prepared J-MOPs could act as an effective photosensitizing agent for enhancing intracellular ROS generation upon 670 nm laser irradiation. Next, the antitumor effect of J-MOPs was investigated. After HepG2 cells were incubated with J-MOPs and exposed to 670 nm laser irradiation, the cells were stained with PI to directly visualize dead cells according to our previously reported protocol.[12,28,44,45] As shown in Fig. 4C, only background red fluorescence was observed in the cells treated with PBS alone or BPQDs (20 μg mL^{-1}) or J-MOPs (BPQDs, 20 μg mL^{-1}) without laser irradiation. Similarly, the cells treated with PBS alone upon 670 nm laser irradiation

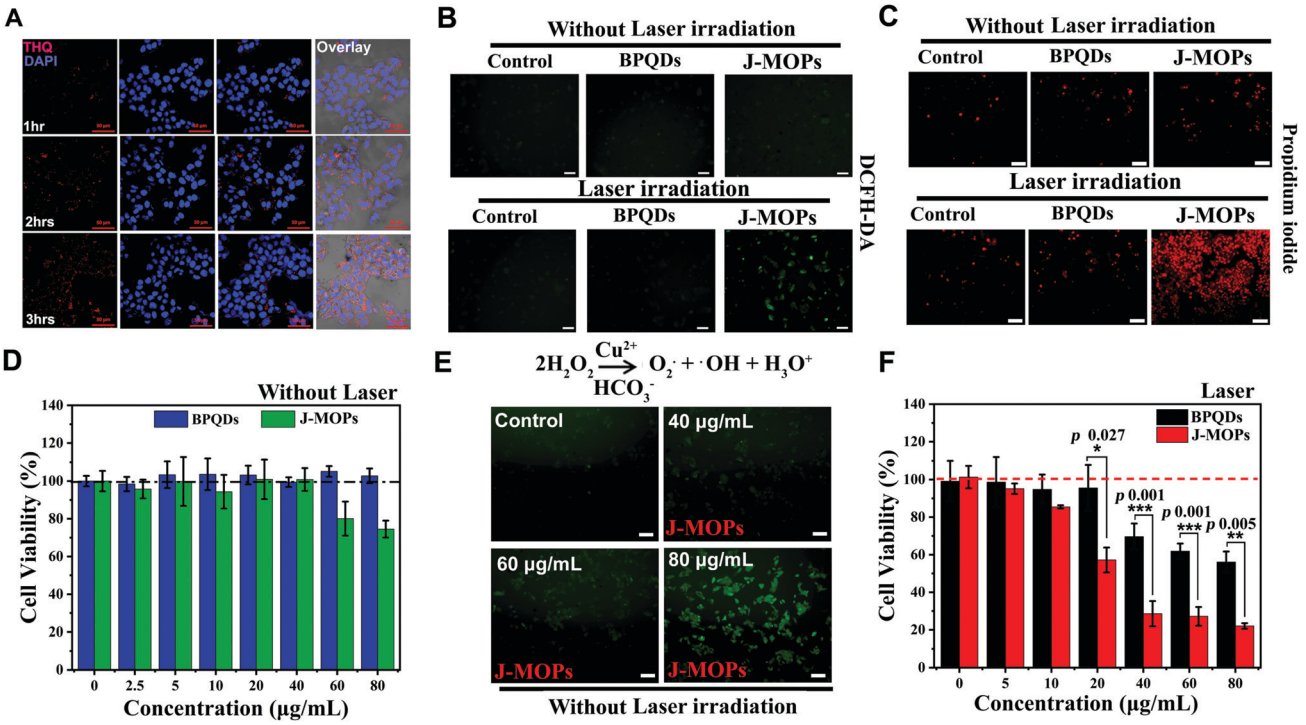

Fig. 4 (A) CLSM images of HepG2 cells treated with the J-MOPs for different incubation times. (B) DCFH-DA detection of HepG2 cells treated with PBS, BPQDs, and J-MOPs with or without 670 nm laser irradiation (0.1 W cm^{-2}, 5 min; scale bars, 200 μm). (C) Corresponding fluorescence images (scale bars, 50 μm) of treated cells stained with PI (dead cells, red fluorescence). (D) Relative cell viability of HepG2 cells after incubation with BPQDs or J-MOPs for 24 h (BPQDs, from 2.5 to 80 μg mL^{-1}). (E) DCFH-DA detection of HepG2 cells treated with J-MOPs at different concentrations (scale bars, 50 μm). (F) Cell viability of HepG2 cells after incubation with different concentrations of BPQDs or J-MOPs for 3 h, and then irradiation with a 670 nm laser (0.1 W cm^{-2}) for 5 min. Statistical analysis was performed using two-tailed paired Student's *t*-tests (**$p < 0.01$, ***$p < 0.001$, and ****$p < 0.0001$).

showed only background levels of red fluorescence. However, significantly more dead cells were observed in J-MOPs-treated HepG2 cells after 670 nm laser irradiation compared with the BPQDs-treated cells subjected to the same laser irradiation conditions or any other groups. To further quantitatively analyze the antitumor effect of our J-MOPs, CCK8 assays were conducted. The cytotoxicity of J-MOPs without laser irradiation was evaluated first. As shown in Fig. 4D and Fig. S6 (ESI†), after incubation with different concentrations of J-MOPs (calculated by BPQDs) for 24 h, the HepG2 cell viabilities of J-MOPs-treated cells remained higher than 95%, even up to 40 μg mL^{-1}, which was comparable with that of bare BPQDs-treated cells. The results were similar for the toxicity of J-MOPs-treated normal liver cells (LO2). However, when the J-MOPs concentration was increased above 60 μg mL^{-1}, our J-MOPs showed certain cytotoxicity, even without laser irradiation (for example, 25.5% of cell growth inhibition at 80 μg mL^{-1} in HepG2; and 11.5% of cell growth inhibition in LO2), which might be due to acid-triggered cleavage of the coordination bonds between P–Cu and Cu–THQ, followed by Cu^{2+} release as a Fenton-like agent for ROS generation from endogenous H_2O_2.[42–44] To prove this assumption, Cu^{2+} release from J-MOPs under tumor-specific acidic conditions (pH 6.5) was investigated. As shown in Fig. S7 (ESI†), 20.6% of Cu^{2+} was released from the J-MOPs after 48 h incubation at pH 6.5, indicating that the J-MOPs could slowly release Cu^{2+} into tumor acidic environments. J-MOPs acting as Fenton-like agents for ROS generation in endogenous H_2O_2 was further confirmed by examining intracellular ROS generation under dark conditions. As shown in Fig. 4E, the green fluorescence intensity of DCFH-DA in J-MOPs-treated cells increased in a concentration-dependent manner, suggesting that the Cu^{2+} ions from degraded J-MOPs could induce severe oxidative stress inside cells. Furthermore, the cell viability of J-MOPs-treated HepG2 cells under 670 nm laser irradiation (0.1 W cm^{-2}, 5 min) was significantly decreased to 22% at 80 μg mL^{-1}, while the bare BPQDs-treated cells retained 56.1% cell viability under the same laser irradiation conditions, suggesting that our J-MOPs had a dramatically enhanced ROS generation ability and PDT efficiency *in vitro* (Fig. 4F).

To further investigate the antitumor tumor effects of our J-MOPs *in vivo*, HepG2 tumor-bearing nude mice received different treatments, as mentioned in the Experimental section (ESI†), and the tumor volumes were measured using a Vernier caliper every 2 days. As shown in Fig. 5A, the mice treated with PBS either with or without laser irradiation experienced rapid tumor growth, indicating that NIR laser irradiation under these power conditions alone had no influence on tumor growth. Although mice treated with BPQDs showed some tumor growth delay when irradiated with a 670 nm laser, the tumors still showed relatively rapid growth. Notably, the mice treated with J-MOPs in the dark (without laser irradiation) showed certain tumor growth delay, due to Cu^{2+} released from J-MOPs as a

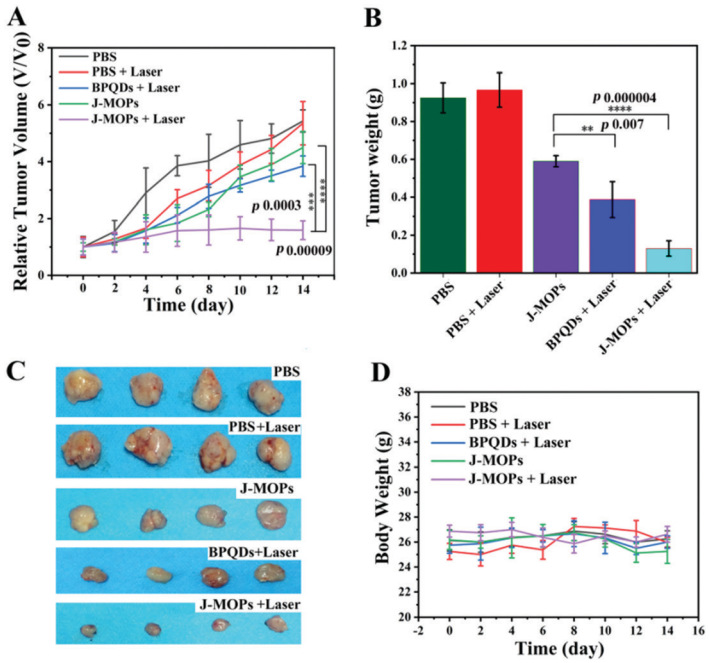

Fig. 5 (A) Tumor volumes of mice with indicated treatments (n = 4). Statistical analysis was performed using two-tailed paired Student's t-tests (***$p < 0.001$, ****$p < 0.0001$). (B) Tumor weight of *ex vivo* tumors after indicated treatments. Statistical analysis was performed using two-tailed paired Student's t-tests (**$p < 0.01$, ****$p < 0.0001$). (C) Photograph of *ex vivo* tumors after indicated treatments at day 14. (D) Mean body weights of mice after indicated treatments.

Fenton-like agent against tumor growth. More obviously, mouse tumors treated with J-MOPs under 670 nm laser irradiation showed the strongest tumor growth inhibition due to an enhanced PDT efficiency and synergy with the Fenton-like activity of Cu^{2+} against tumors. To further confirm these results *in vivo*, *ex vivo* fresh tumors were crushed, centrifuged, and incubated with J-MOPs with or without 670 nm laser irradiation (0.1 W cm^{-2}, 5 min). The $^{\bullet}$OH from the tumor microenvironment H_2O_2 and total ROS from J-MOPs upon 670 nm laser irradiation were determined using TMB and DCFH-DA probes, respectively.[46] As shown in Fig. S8 (ESI†), the TMB absorbance of J-MOPs under dark conditions was much higher than that of the control under the

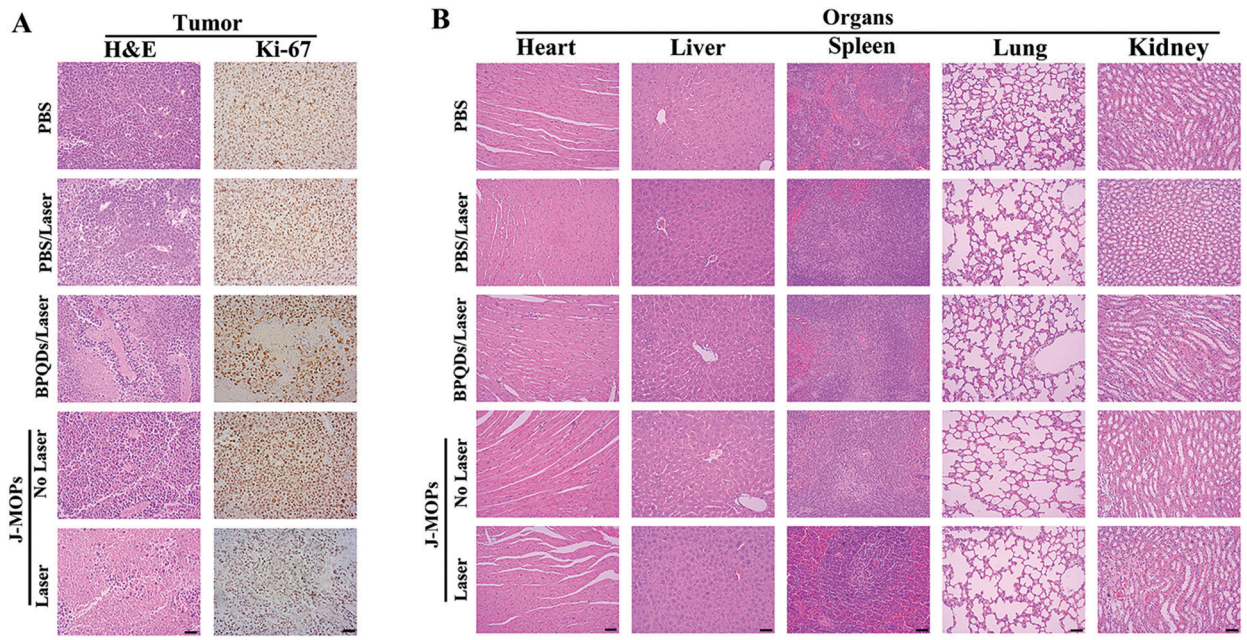

Fig. 6 (A) Corresponding H&E and immuno-histochemical staining of the tumor tissues after 48 h of treatment as indicated (scale bar, 50 μm). (B) Pathological changes in major organs evaluated by H&E staining, acquired at 14 days after different treatments as indicated (scale bar, 50 μm).

same conditions, which was due to Cu^{2+} released from J-MOPs as Fenton-like agents to generate $^{\bullet}OH$ from H_2O_2. In contrast, the DCFH-DA fluorescence intensity of J-MOPs with laser irradiation was obviously higher than that of J-MOPs in the dark and the control groups without laser irradiation, suggesting that the total ROS generation (singlet oxygen ($^1O_2$) and $^{\bullet}OH$) was resulting from J-MOPs upon 670 nm laser irradiation. The additional DCFH-DA fluorescence of J-MOPs in the dark was derived from $^{\bullet}OH$. The therapeutic efficacy was also confirmed by calculating the *ex vivo* tumor weight (Fig. 5B and C), and investigating hematoxylin–eosin (H&E) and immunohistochemical (IHC) (Ki67) staining after 48 h of indicated treatments. As shown in Fig. 6A, the tumors of J-MOPs-treated mice after 670 nm laser irradiation showed typical cytoskeleton collapse and nucleus dissociation. These phenomena were much more serious than BPQDs-treated mice under the same laser irradiation conditions. Additionally, the Ki67 signal in the tumors of J-MOPs-treated mice after laser irradiation was much weaker than that of any other groups, further demonstrating the excellent therapeutic efficacy of our J-MOPs. Finally, the body weight was investigated to roughly evaluate the toxicity of J-MOPs. As shown in Fig. 5D, no significant body-weight loss was observed in mice from any group, suggesting the excellent biocompatibility of our designed J-MOPs. This was further confirmed by H&E staining of the major organs (heat, liver, spleen, lung, and kidney) after the indicated treatments (Fig. 6B). In summary, these results clearly demonstrated that our prepared J-MOPs could serve as an effective photosensitizing agent against tumors with excellent biosafety.

Conclusions

We have reported a novel and simple strategy to fabricate Janus nanoparticles based on BPQDs and THQ–Cu MOPs to simultaneously improve the environmental stability and ROS generation ability of black phosphorus materials for PDT treatment. In this novel nanostructure, the J-MOPs not only protected against BPQDs degradation through effective encapsulation and Cu–P bonds, but also endowed BQPDs with dramatic electron/hole separation and migration abilities to enhance the ROS generation during PDT treatment. Interestingly, the tumor microenvironment-triggered degradation of J-MOPs could release Cu^{2+} ions to serve as Fenton-like agents to further improve the antitumor efficacy by synergizing with PDT. Therefore, we have highlighted the potential of our designed J-MOPs to acts as a promising cancer phototherapy agent for possible clinical applications.

Conflicts of interest

The authors declare no competing financial interests.

Acknowledgements

D. Z. and Z. G. L. contributed equally to this work. This work was supported by the Natural Science Foundation of China (Grant No. 61805041, U1505221, 61727823, 61875141, and 61575044); the Natural Science Foundation of Fujian Province (Grant No. 2016J01174); the Medical Innovation Project of Fujian province (Grant No. 2018-CX-49); and the Wu Jie-Ping Medical Foundation (Grant No. LDWJPMF-102-17007).

References

1 L. Bai, X. Wang, S. Tang, Y. Kang, J. Wang, Y. Yu, Z. K. Zhou, C. Ma, X. Zhang, J. Jiang, P. K. Chu and X. F. Yu, *Adv. Mater.*, 2018, **30**, 3641.
2 M. Wen, J. Wang, R. Tong, D. Liu, H. Huang, Y. Yu, Z.-K. Zhou, P. K. Chu and X.-F. Yu, *Adv. Sci.*, 2018, 1801321.
3 X. Zhang, H. Xie, Z. Liu, C. Tan, Z. Luo, H. Li, J. Lin, L. Sun, W. Chen, Z. Xu, L. Xie, W. Huang and H. Zhang, *Angew. Chem.*, 2015, **54**, 3653.
4 R. Gui, H. Jin, Z. Wang and J. Li, *Chem. Soc. Rev.*, 2018, **47**, 6795.
5 S. C. Dhanabalan, J. S. Ponraj, Z. Guo, S. Li, Q. Bao and H. Zhang, *Adv. Sci.*, 2017, **4**, 1600305.
6 L. Chan, P. Gao, W. Zhou, C. Mei, Y. Huang, X. F. Yu, P. K. Chu and T. Chen, *ACS Nano*, 2018, **12**, 12401–12415.
7 W. Zhou, T. Pan, H. Cui, Z. Zhao, P. K. Chu and X. F. Yu, *Angew. Chem.*, 2018, **3**, 779.
8 W. Zhou, H. Cui, L. Ying and X. F. Yu, *Angew. Chem.*, 2018, **57**, 10268.
9 J. Shao, C. Ruan, H. Xie, Z. Li, H. Wang, P. K. Chu and X. F. Yu, *Adv. Sci.*, 2018, **5**, 1700848.
10 W. Chen, J. Ouyang, H. Liu, M. Chen, K. Zeng, J. Sheng, Z. Liu, Y. Han, L. Wang, J. Li, L. Deng, Y. N. Liu and S. Guo, *Adv. Mater.*, 2017, **29**, 1603864.
11 W. Tao, X. Zhu, X. Yu, X. Zeng, Q. Xiao, X. Zhang, X. Ji, X. Wang, J. Shi, H. Zhang and L. Mei, *Adv. Mater.*, 2017, **29**, 1802061.
12 D. Zhang, M. Wu, Z. Cai, N. Liao, K. Ke, H. Liu, M. Li, G. Liu, H. Yang, X. Liu and J. Liu, *Adv. Sci.*, 2018, **5**, 1700648.
13 M. Liu, L. Wang, X. Zheng, S. Liu and Z. Xie, *ACS Appl. Mater. Interfaces*, 2018, **10**, 24638.
14 D. Zhang, A. Zheng, J. Li, M. Wu, L. Wu, Z. Wei, N. Liao, X. Zhang, Z. Cai, H. Yang, G. Liu, X. Liu and J. Liu, *Theranostics*, 2017, **7**, 164.
15 L. Wang, M. Huo, Y. Chen and J. Shi, *Adv. Healthcare Mater.*, 2018, **7**, 1701156.
16 Z. Guo, S. Chen, Z. Wang, Z. Yang, F. Liu, Y. Xu, J. Wang, Y. Yi, H. Zhang, L. Liao, P. K. Chu and X. F. Yu, *Adv. Mater.*, 2017, **29**, 1703811.
17 Y. Zhao, L. Tong, Z. Li, N. Yang, H. Fu, L. Wu, H. Cui, W. Zhou, J. Wang, H. Wang, P. K. Chu and X.-F. Yu, *Chem. Mater.*, 2017, **29**, 7131–7139.
18 Z. Sun, Y. Zhao, Z. Li, H. Cui, Y. Zhou, W. Li, W. Tao, H. Zhang, H. Wang, P. K. Chu and X.-F. Yu, *Small*, 2017, **13**, 1602896.
19 L. Wu, J. Wang, J. Lu, D. Liu, N. Yang, H. Huang, P. K. Chu and X. Yu, *Small*, 2018, **29**, 1801405.
20 Y. Zhao, H. Wang, H. Huang, Q. Xiao, Y. Xu, Z. Guo, H. Xie, J. Shao, Z. Sun, W. Han, X. F. Yu, P. Li and P. K. Chu, *Angew. Chem.*, 2016, **55**, 5003.

21 X. Zeng, M. Luo, G. Liu, X. Wang, W. Tao, Y. Lin, X. Ji, L. Nie and L. Mei, *Adv. Sci.*, 2018, **5**, 1800510.
22 H. Wang, K. Hu, Z. Li, C. Wang, M. Yu, Z. Li and Z. Li, *Small*, 2018, **14**, 1801701.
23 R. Gusmao, Z. Sofer and M. Pumera, *ACS Nano*, 2018, **12**, 5666.
24 S. T. Han, L. Hu, X. Wang, Y. Zhou, Y. J. Zeng, S. Ruan, C. Pan and Z. Peng, *Adv. Sci.*, 2017, **4**, 1600435.
25 W. Chen, J. Ouyang, X. Yi, Y. Xu, C. Niu, W. Zhang, L. Wang, J. Sheng, L. Deng, Y. N. Liu and S. Guo, *Adv. Mater.*, 2018, **30**, 1703458.
26 M. Qiu, D. Wang, W. Liang, L. Liu, Y. Zhang, X. Chen, D. K. Sang, C. Xing, Z. Li, B. Dong, F. Xing, D. Fan, S. Bao, H. Zhang and Y. Cao, *Proc. Natl. Acad. Sci. U. S. A.*, 2018, **115**, 501.
27 J. Shao, H. Xie, H. Huang, Z. Li, Z. Sun, Y. Xu, Q. Xiao, X. F. Yu, Y. Zhao, H. Zhang, H. Wang and P. K. Chu, *Nat. Commun.*, 2016, **7**, 12967.
28 D. Zhang, X. Lin, S. Lan, H. Sun, X. Wang, X. Liu, Y. Zhang and Y. Zeng, *Part. Part. Syst. Charact.*, 2018, **35**, 1800010.
29 H. Zhang, H. Li, H. Fan, J. Yan, D. Meng, S. Hou, Y. Ji and X. Wu, *Nano Res.*, 2018, **11**, 1456.
30 F. He, G. Chen, Y. Yu, S. Hao, Y. Zhou and Y. Zheng, *ACS Appl. Mater. Interfaces*, 2014, **6**, 7171.
31 J. Chen, C. L. Dong, D. Zhao, Y. C. Huang, X. Wang, L. Samad, L. Dang, M. Shearer, S. Shen and L. Guo, *Adv. Mater.*, 2017, **29**, 1606198.
32 W. He, H. K. Kim, W. G. Wamer, D. Melka, J. H. Callahan and J. J. Yin, *J. Am. Chem. Soc.*, 2013, **136**, 750–757.
33 G. Song, M. Chen, Y. Zhang, L. Cui, H. Qu, X. Zheng, M. Wintermark, Z. Liu and J. Rao, *Nano Lett.*, 2018, **18**, 182.
34 Y. Ju, H. Zhang, J. Yu, S. Tong, N. Tian, Z. Wang, X. Wang, X. Wang, X. Su, X. Chu, J. Lin, Y. Ding, G. Li, F. Sheng and Y. Hou, *ACS Nano*, 2017, **11**, 9239.
35 J. Song, B. Wu, Z. Zhou, G. Zhu, Y. Liu, Z. Yang, L. Lin, G. Yu, F. Zhang, G. Zhang, H. Duan, G. Stucky and X. Chen, *Angew. Chem.*, 2017, **129**, 8222.
36 Y. H. Zhu, X. Yang, D. Bao, X. F. Bie, T. Sun, S. Wang, Y. S. Jiang, X. B. Zhang, J.-M. Yan and Q. Jiang, *Joule*, 2018, **2**, 736–746.
37 Q. Zhang, H. Zhong, F. Meng, D. Bao, X. Zhang and X. Wei, *Nano Res.*, 2018, **11**, 1294–1300.
38 S. Yuan, S. Wang, L. Li, Y. H. Zhu, X. B. Zhang and J. M. Yan, *ACS Appl. Mater. Interfaces*, 2016, **8**, 9178–9184.
39 M. M. Shi, D. Bao, B. R. Wulan, Y. H. Li, Y. F. Zhang, J. M. Yan and Q. Jiang, *Adv. Mater.*, 2017, **29**, 1606550.
40 X. Chen, N. Li, Z. Kong, W.-J. Ong and X. Zhao, *Mater. Horiz.*, 2018, **5**, 9–27.
41 D. Bao, Q. Zhang, F. L. Meng, H. X. Zhong, M. M. Shi, Y. Zhang, J. M. Yan, Q. Jiang and X. B. Zhang, *Adv. Mater.*, 2017, **29**, 1604799.
42 D. Zhang, H. Xu, X. Zhang, Y. Liu, M. Wu, J. Li, H. Yang, G. Liu, X. Liu, J. Liu and Z. Yuan, *ACS Appl. Mater. Interfaces*, 2018, **10**, 25203.
43 M. F. Poyton, A. M. Sendecki, X. Cong and P. S. Cremer, Cu^{2+} Binds to Phosphatidylethanolamine and Increases Oxidation in Lipid Membranes, *J. Am. Chem. Soc.*, 2016, **138**, 1584.
44 C. He, D. Liu and W. Lin, *Chem. Rev.*, 2015, **115**, 11079.
45 D. Zhang, Z. Cai, N. Liao, S. Lan, M. Wu, H. Sun, Z. Wei, J. Li and X. Liu, *Chem. Sci.*, 2018, **9**, 7390.
46 A. Üzer, S. Durmazel, E. Erçağ and R. Apak, *Sens. Actuators, B*, 2017, **247**, 98.